DISCLAIMER

This report was prepared as an account of work sponsored by an agency of the United States Government. Neither the United States Government nor any agency thereof, nor any of their employees, makes any warranty, express or implied, or assumes any legal liability or responsibility for the accuracy, completeness, or usefulness of any information, apparatus, product, or process disclosed, or represents that its use would not infringe privately owned rights. Reference herein to any specific commercial product, process, or service by trade name, trademark, manufacturer, or otherwise does not necessarily constitute or imply its endorsement, recommendation, or favoring by the United States Government or any agency thereof. The views and opinions of authors expressed herein do not necessarily state or reflect those of the United States Government or any agency thereof. Reference herein to any social initiative (including but not limited to Diversity, Equity, and Inclusion (DEI); Community Benefits Plans (CBP); Justice 40; etc.) is made by the Author independent of any current requirement by the United States Government and does not constitute or imply endorsement, recommendation, or support by the United States Government or any agency thereof.

LLNL-SR-2002065

Lawrence Livermore National Laboratory

Quasi-static to Dynamic Mechanical Response and Microstructure Development of Tantalum-Tungsten Alloys

N. Peterson, C. Smith, E. Pittman, L. Lamberson, K. Clarke, A. Clarke

January 2025

Quasi-static to Dynamic Mechanical Response and Microstructure Development of Tantalum-Tungsten Alloys

Nate Peterson, Charles Smith, Emily Pittman, Leslie Lamberson, Kester Clarke, Amy Clarke

Metallurgical and Materials Engineering
Colorado School of Mines

Prepared by LLNL under Contract DE-AC52-07NA27344.

1 Introduction

1.1 Motivation

Lawrence Livermore National Laboratory (LLNL) is interested the quasi-static to dynamic mechanical response and microstructure evolution of tantalum-tungsten (Ta-W) alloys (Ta-2.5W, Ta-5W, and Ta-10W, wt.%) made by conventional wrought processing and additive manufacturing (AM). This work scope was performed at the Colorado School of Mines (Mines) and included quasi-static (e.g., 10^{-3} s^{-1}) mechanical testing in tension and compression, along with selected high strain rate (Kolsky) pressure bar testing in compression (e.g., 10^{3} s^{-1}), with and without temperature variations in some instances. Complementary microstructure characterization was performed on undeformed and deformed samples to understand the role of processing on microstructural evolution and the deformation mechanisms that impact the mechanical response with variations in strain rate, temperature, and strain state (e.g., tension versus compression in selected examples). The wrought material provided by LLNL from Viridis Materials was found to have unrecrystallized regions within the microstructure, which led to unexpected results relative to previously reported properties for Ta-W. The AM Ta-2.5W (wt.%) material provided by LLNL was found to have higher compressive strength than wrought Ta-2.5W (wt.%), which is hypothesized to be due to differences in the crystallographic texture between the two materials. This project partially supported several postdocs and graduate students at Mines.

1.2 FY24 Accomplishments

In FY24, we made progress in following areas:

- Obtained wrought Ta-2.5W, Ta-5W and Ta-10W (wt.%) plate materials from Viridis Materials (VM) via LLNL and performed microstructure characterization these materials.
- Performed baseline mechanical testing (compression and tension) of the wrought plate materials at different strain rates, ranging from 10^{-3} up to 10^{3} and at temperatures up to 500 °C. Under high-rate compression conditions, it was found that increasing W resulted in increasing yield and flow stresses.
- Developed an improved, high temperature testing setup in the Gleeble 3500 for thermomechanical deformation with combined digital image correction (DIC) and infrared (IR) thermal imaging for testing at different strain rates and temperatures.

- Obtained additively manufactured Ta-2.5W (wt.%) material from LLNL for characterization and testing.
- Performed room temperature compression and tension testing of AM Ta-2.5W (wt.%) material along and transverse to the build direction (BD). Experiments were conducted at strain rates ranging between 10^{-3} and 10^{3} s^{-1}. In compression, the AM Ta-2.5W demonstrated a higher yield stress than the wrought material, when tested along both the build and transverse directions. In tension, the material was found to have reduced ductility when compared to the wrought material.

2 Wrought Ta-W alloy plate characterization (quasi-static)

Wrought Ta-W alloy plates (Ta-2.5W, Ta-5W, and Ta-10W, wt.%) were provided to Mines by LLNL for microstructural characterization and baseline mechanical testing. The wrought plates were given in two dimensions; 6" x 6" x ½" or 6" x 6" x 1/8". Ta-2.5W and Ta-5W plates were supplied by VM, while the Ta-10W plate was legacy material from LLNL. The pedigree of the Ta-10W material is unknown. Additional samples machined from Ta-2.5W and Ta-5W material supplied by American Elements were also provided to Mines for testing. The source of the materials are noted in the results where appropriate.

2.1 Experimental approach

2.1.1 Characterization

For each alloy, a through-thickness cross-section from one of the provided ½" plates was sectioned and mounted for metallography and microstructure characterization. The plate material was inspected with light optical microscopy (LOM) and electron microscopy (secondary electron (SE), backscattered electron (BSE), and electron backscatter diffraction (EBSD)) to characterize grain structures and orientations. The samples were polished using standard metallographic procedures; increasingly fine SiC papers were used for rough sample grinding (220 – 1200 grit), followed by polishing with alumina suspensions at 3 μm and 0.3 μm on a woven polishing pad (LECO Imperial). For optical microscopy the samples were etched to reveal the grain boundaries using an immersion etch of 6 mL HNO_3 and 1 mL HF for approximately 40 s. For electron microscopy the samples were repolished with a final step using colloidal silica for 12 h. Samples of each alloy were sent out to an external lab for compositional analysis to measure interstitial contents (C, N, O) using combustion and inert gas fusion techniques. The C, N, and O contents in the three wrought materials are provided in Table 2.1. For each of the alloys, the bulk W composition was found to be within 0.1 wt.% of the nominal composition.

Table 2.1: Measured C, N, and O contents in the wrought Ta-2.5W, Ta-5W and Ta-10W plate materials investigated in this study. The concentrations are listed in ppmw.

	Ta-2.5W (VM)	Ta-5W (VM)	Ta-10W (VM)
C	20	10	<100
N	15	10	<100
O	70	85	<100

2.1.2 Mechanical testing

Mechanical testing was performed at Mines using a variety of load frames, including servohydraulic (Gleeble 3500) and electromechanical (Alliance RT/100, Mark-10) frames, depending upon the testing

requirements for strain rate and/or temperature. Elevated temperature, uniaxial compression and tension testing was performed with a Gleeble 3500 thermo-mechanical simulator at various strain rates (10^{-3} – 10^{1} s^{-1}). Samples for mechanical testing were electro-discharge machined (EDM) from the wrought plates. For compression testing two distinct sample geometries were used, namely 6 x 9 mm and 5 x 5 mm (diameter, height). The smaller compression geometry was used later in the project to match the geometry used for the high strain rate compression testing (Section 3). The 6 x 9 mm geometry was used for the elevated temperature testing. K-type thermocouples were utilized for all tests at temperatures up to 1000 °C.

Tension testing was performed on two distinct sample geometries, a standard subsize E8 geometry [1] and a miniature geometry derived from the subsize E8 standard. The miniature tensile bar geometry is shown in Figure 2.1. This geometry was optimized using an iterative design process using steady-state, thermal-electric finite element analysis (FEA) simulations with Ansys Mechanical. An ideal gage section of 10 mm was chosen, based upon the availability of a high temperature extensometer. The primary factor in determining the temperature gradient across the gage section was the overall gage section width. It should be noted that other modifications to the test setup, primarily the wedge setup, have been demonstrated in the literature to help improve (i.e., reduce) the temperature gradient across the sample gage section [2]. The thermal gradient was confirmed by thermocouples placed at 5 and 7 mm from the center of the total gage section. The temperature loss from the absolute center at the 5 mm position (10 mm sub-gage) was approximately 3%.

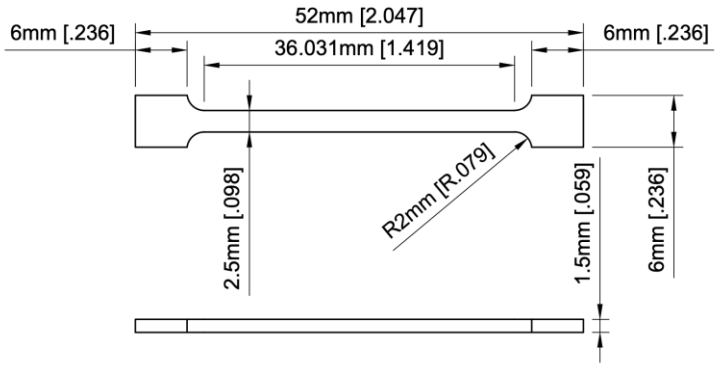

Figure 2.1: Miniature tensile bar sample dimensions. This design was derived from the subsize E8 standard (ASTM-E8) and optimized to provide a 10 mm gage length at the center of the total gage length that has a minimal temperature gradient.

2.1.2.1 High temperature extensometer

Gleeble thermomechanical simulators utilize resistive sample heating to enable rapid heating rates, however this typically results in a significant thermal gradient across the sample gage section. At Mines, there is a high temperature extensometer available for use with the Gleeble, which has a 10 mm nominal gage length. However, it was found during use that the extensometer was not a reliable strain measurement device, due to the inability to set a fixed zero position and because of additional stresses placed on the sample associated with the mounting bands that secure the ceramic rods to the sample. After initial tests were performed with the extensometer, a switch to using digital image correlation (DIC) in conjunction with infrared (IR) thermal imaging was made to enable the measurement of strains and thermal gradients across the sample, respectively.

2.1.2.2 Combined DIC and IR thermal imaging camera setup

The configuration with the DIC and the IR thermal camera setup on the Gleeble thermomechanical simulator is shown in Figure 2.2. The DIC configuration used was 2D (single camera). The optical camera used for the DIC measurements was a Basler acA3800-14um digital camera. For thermal imaging, an Optris PI 640i IR camera was used, which utilizes the mid-infrared range (λ = 8-14 μm). To enable the IR camera to view the sample, a commercially available IR window glass (Fluke FLK-075-CLKT) was purchased and repurposed to fit inside viewports on the Gleeble sample chamber. These viewports are approximately 3" in diameter and are normally utilized with a laser extensometer. This IR window is made of CaF_2, which is nominally transparent to infrared radiation up to ~12 μm [3]. To prevent damage to the IR window, an aluminum backing plate was made from 3" OD, 1" ID tube and Viton gaskets. Both cameras were triggered to start manually after starting a Gleeble test procedure.

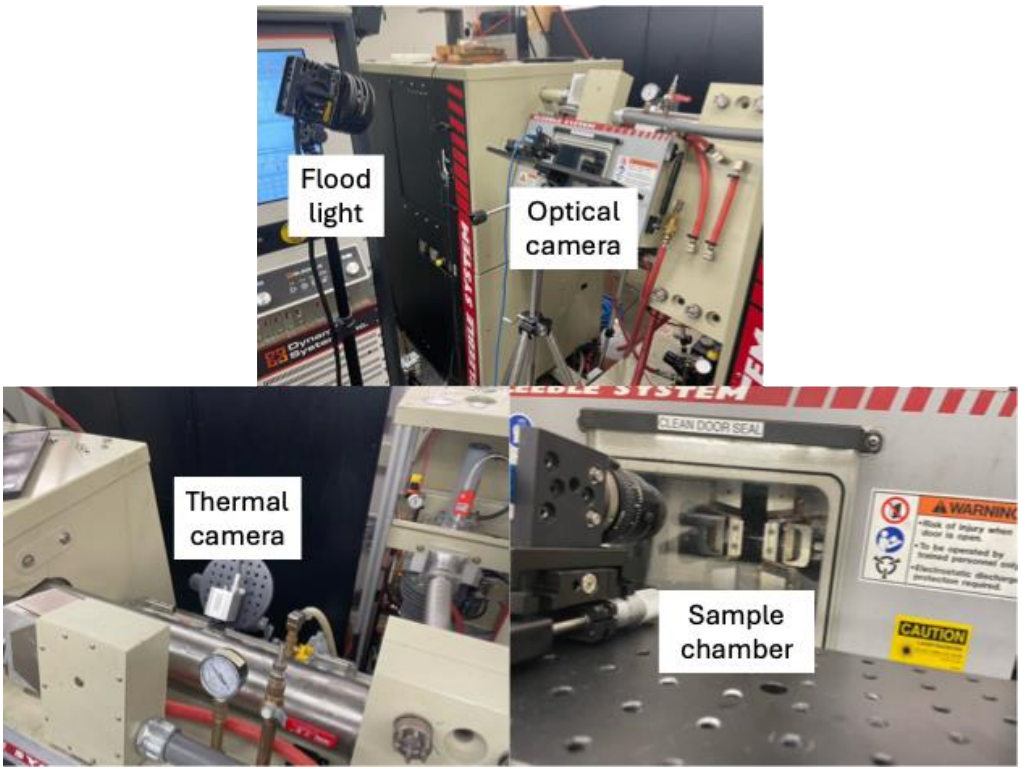

Figure 2.2: Layout of the combined optical (DIC) and thermal imaging camera setup on the Gleeble 3500 at Mines.

The samples were prepared for DIC and thermal imaging by first grinding away the residual recast layer from the EDM process using 1200 grit SiC paper, followed by cleaning with isopropyl alcohol. A base layer of white, high temperature ceramic-based spray paint was applied and allowed to dry, followed by careful application of the speckle pattern using black high temperature ceramic-based spray paint. An alternative method of using Y_2O_3 spray directly on the as-EDM'd surface was also evaluated, but the high temperature spray paint was found to be sufficient for the temperature regimes tested in this work (maximum of 500 °C).

2.2 Results/Outcomes

2.2.1 As-received wrought plate microstructures

The microstructures of the as-received wrought plates are shown in Figure 2.3. There was evidence of unrecrystallized regions found in both the Ta-2.5W and Ta-5W ½" thick plate material. The Ta-2.5W material appeared to contain the highest fraction of unrecrystallized regions, although semi-equiaxed regions were observed in both plates. The legacy Ta-10W plate material also showed evidence of unrecrystallized regions, however most of the plate cross-section was found to be recrystallized. These observations were made from a single ½" plate from each of the three alloys, from which mechanical test samples were also machined.

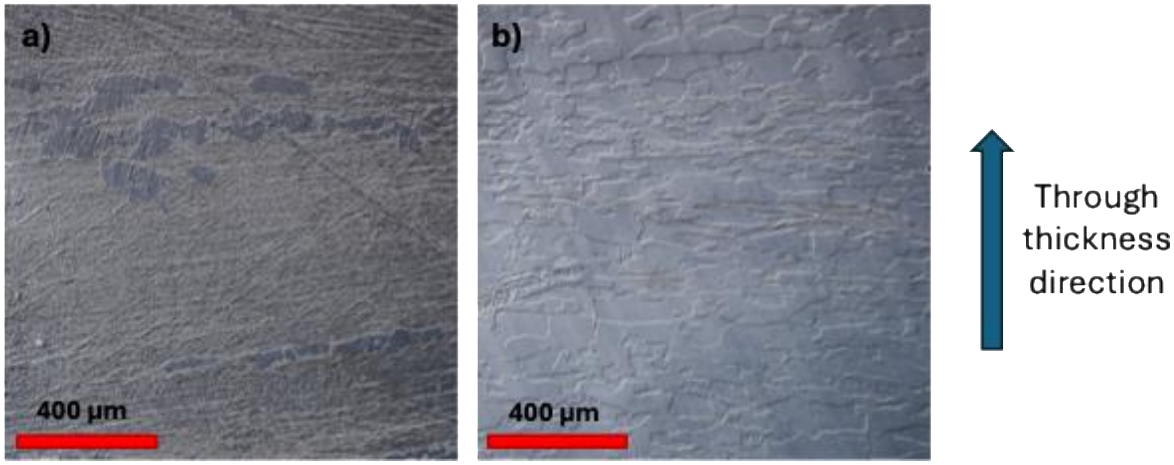

Figure 2.3: Etched micrographs of the as-received microstructure in a) Ta-2.5W wrought plate (1/2") and b) Ta-5W wrought plate. The presence of unrecrystallized bands/regions is evident in both samples, particularly in the Ta-2.5W material sourced from VM.

Inverse pole figure (IPF) maps of equiaxed regions in the Ta-2.5W and Ta-5W ½" plate materials are shown in Figure 2.4. While the maps were collected over a relatively small area (~ 1 x 1 mm), the macrotexture estimated from these maps are both <100> fibers, with the <100> poles aligned along the rolling direction (RD), which is consistent with previous reports of wrought Ta-W alloy plate macrotextures [4,6]. The average grain size estimated from these maps for the recrystallized regions is 47 $\pm$ 29 µm (954 grains) and 41 $\pm$ 29 µm (1145 grains), for the Ta-2.5W and Ta-5W, respectively.

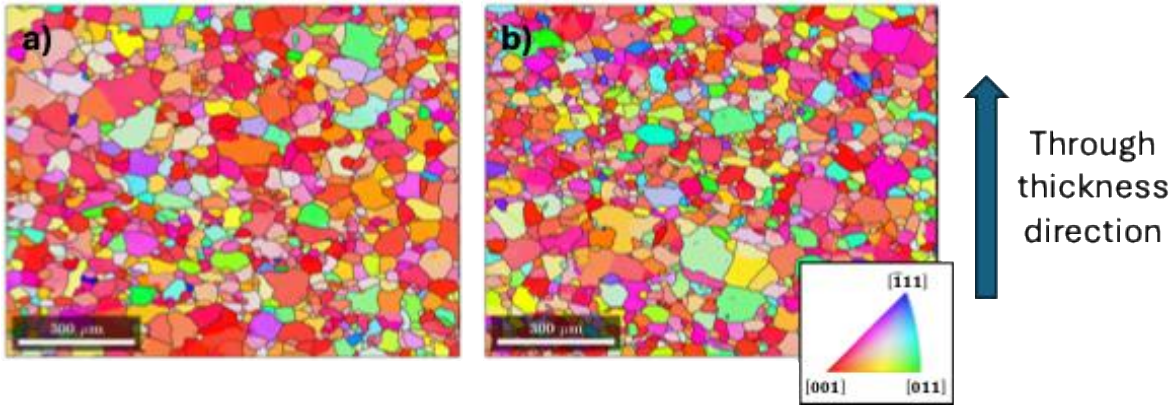

Figure 2.4: Inverse pole figure (IPF) maps of the as-received microstructure in a) Ta-2.5W wrought plate (1/2") and b) Ta-5W wrought plate. The IPF maps are aligned to show the crystal orientation with respect to the RD. This material was sourced from VM.

2.2.2 Compression test results

Uniaxial compression stress/strain curves collected at room temperature and quasi-static and intermediate strain rates are shown in Figure 2.5 for all three wrought Ta-W alloys studied in this work.

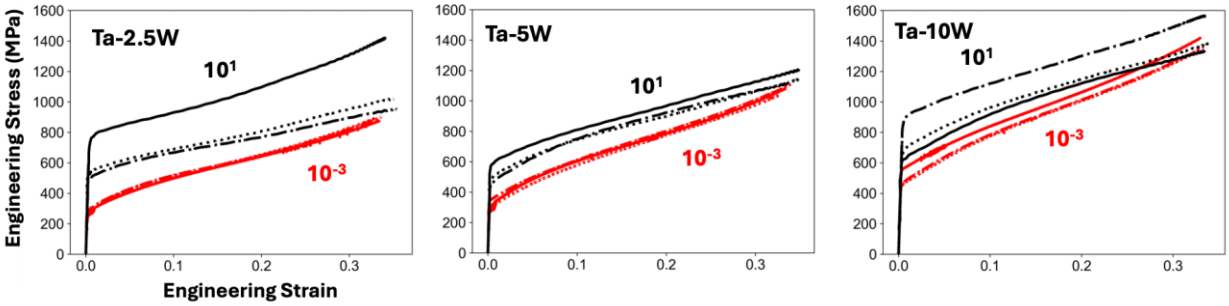

Figure 2.5: Engineering compressive stress/strain plots for all three alloys tested in this work at two strain rates, 10^{-3} s^{-1} (red) and 10^{1} s^{-1} (black) at room temperature. A few of the tests appear to be significant outliers, particularly in the 10^{1} s^{-1} tests. The Ta-2.5W and Ta-5W material was sourced from VM.

2.2.3 Tension test results

2.2.3.1 Effects of strain rate on mechanical response

The effect of strain rate was investigated as a separate variable from the effects of temperature on the mechanical behavior of the three wrought Ta-W alloys. Engineering stress/strain curves obtained from uniaxial tension testing performed at room temperature are shown in Figure 2.6. The presence of yield point elongation (YPE) (discontinuous yielding) is evident, which is dependent on strain rate. YPE is commonly associated with small amounts of interstitials or substitutional impurities. In most cases, the applied stress is inversely proportional to the density of mobile dislocations (defects). As the impurities pin dislocations, the applied stress must increase until the point where the dislocation can break free, causing the load drop. This process is strain rate dependent, as seen in Figure 2.6; at relatively fast strain rates (10^{-1} s^{-1}), the YPE becomes more pronounced as dislocations are pinned at a much higher rate. However, at slower strain rates (10^{-5} s^{-1}), the dislocations are pinned much slower, allowing the material

to move past the yield point without experiencing a YPE phenomenon.

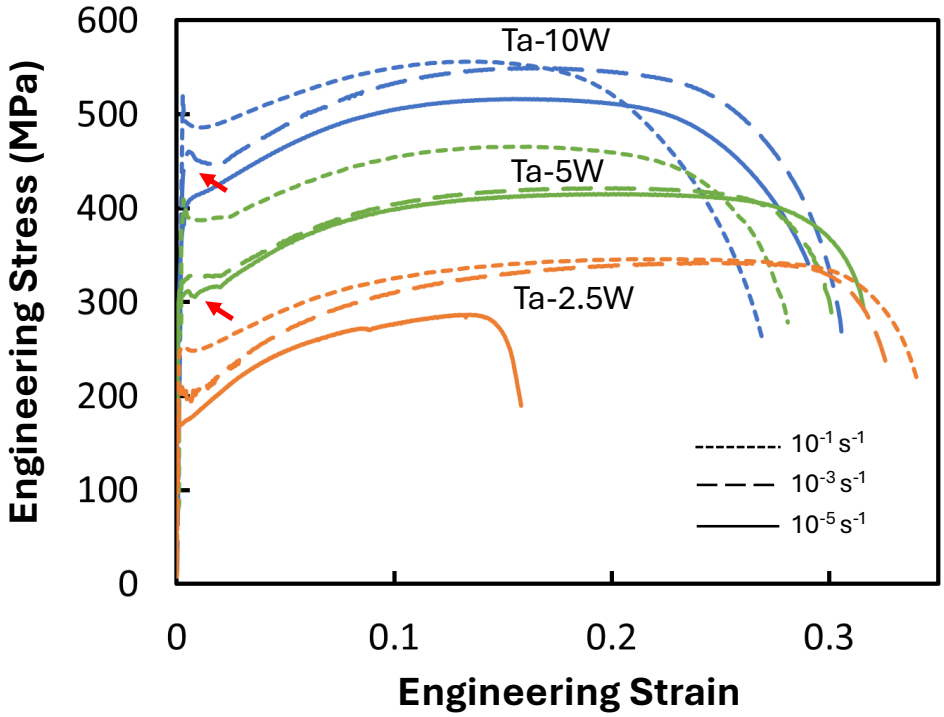

Figure 2.6: Engineering tensile stress/strain plots for all three Ta-W alloys tested in uniaxial tension at three strain rates (approximately quasi-static) at room temperature. The presence of yield-point elongation (YPE), example regions indicated with red arrows, is evident in all three alloys, particularly when comparing the tests run at 10^{-5} vs 10^{-3} s^{-1}. The Ta-2.5W and Ta-5W material was sourced from VM. These tests used the subsize E8 standard sample geometry.

Additional tests were performed on the Ta-2.5W and Ta-5W materials at higher strain rates to complement the initial test tensile test performed on the wrought Ta-10W. (Figure 2.7). The strain rates tested were expanded to include 1 and 10 s^{-1}.

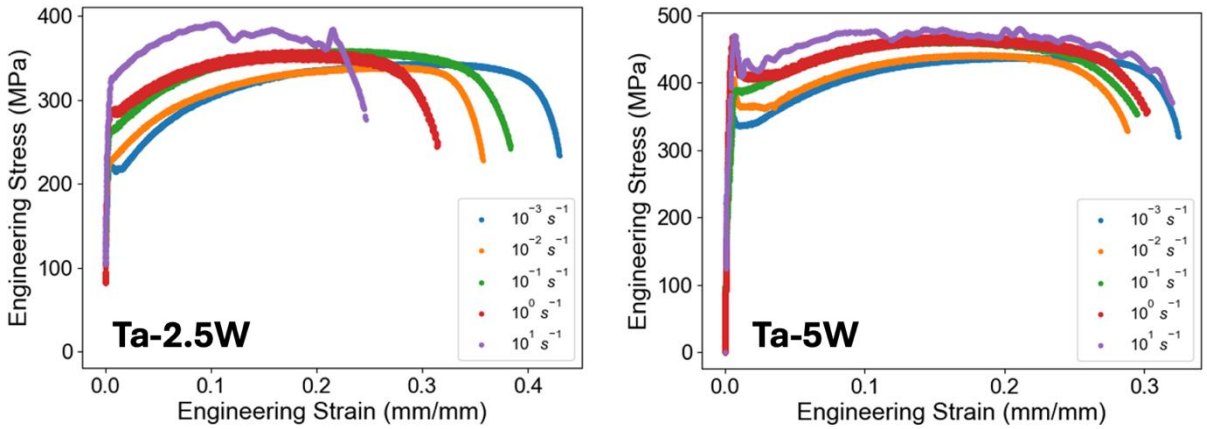

Figure 2.7: Engineering stress/strain plots for the Ta-2.5W and Ta-5W material (VM) tested in uniaxial tension across five decades of strain rate at room temperature. These tests used the subsize E8 sample geometry.

Interrupted strain testing was conducted on Ta-10W tensile samples to observe the microstructure evolution. Three samples were strained at a quasistatic strain rate (10^{-3} s^{-1}), and the tests were aborted at 2%, 8%, and 16% elongation. Samples were collected from the uniformed deformed gage length, and EBSD was performed to observe the evolution of the microstructure. Grain Reference Orientation Deviation (GROD) maps were constructed, as shown in Figure 2.8. With increasing deformation, there is an increase in the average misorientation present in each map. The increase in misorientation can be correlated to an increase in dislocation pile up at grain boundaries. There are also traces of subgrains or recrystallized grains that form, which can be identified as small grains with low internal misorientations. However, due to the presence of unrecrystallized regions in the wrought material, when these small grains form remains unclear.

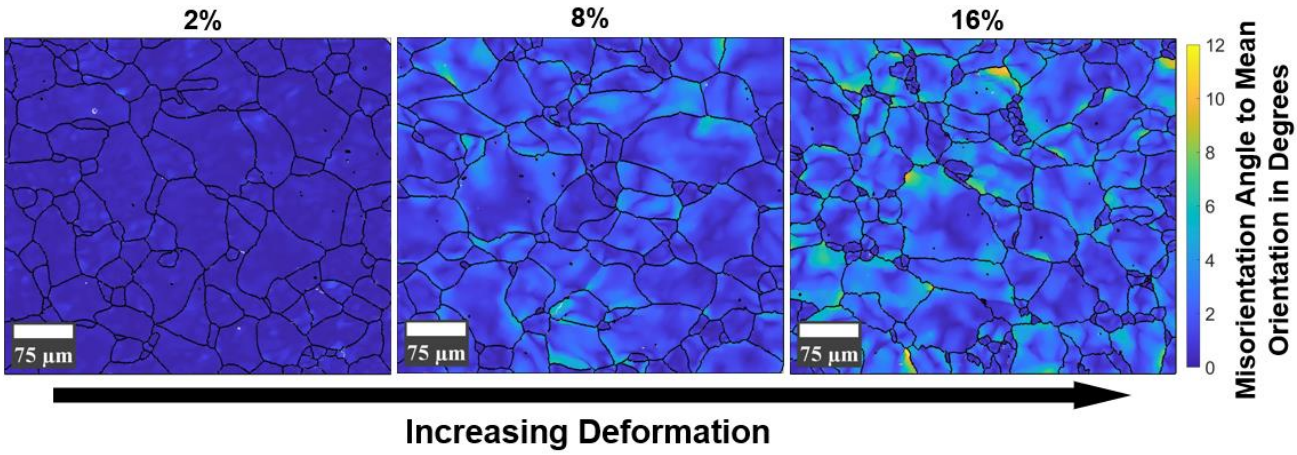

Figure 2.8: GROD maps of Ta-10W tensile samples with increasing deformation.

2.2.3.1 Effects of temperature on mechanical response

Unixaial tension stress/strain curves as a function of temperature (up to 500 °C) in Ta-2.5W and Ta-10W are shown in Figure 2.9. These tests utilized the combined DIC/thermal imaging configuration. The yielding behavior is distinct in the Ta-2.5W at all temperatures compared to the results obtained for the Ta-10W. Both alloys show some level of temperature dependence on yield strength, but the trend is much clearer in the Ta-10W material. The strain hardening rate behavior also appears to change at higher temperatures (> 400 °C) in the Ta-10W, which is an expected behavior of body centered cubic (BCC) metals and alloys at elevated temperatures.

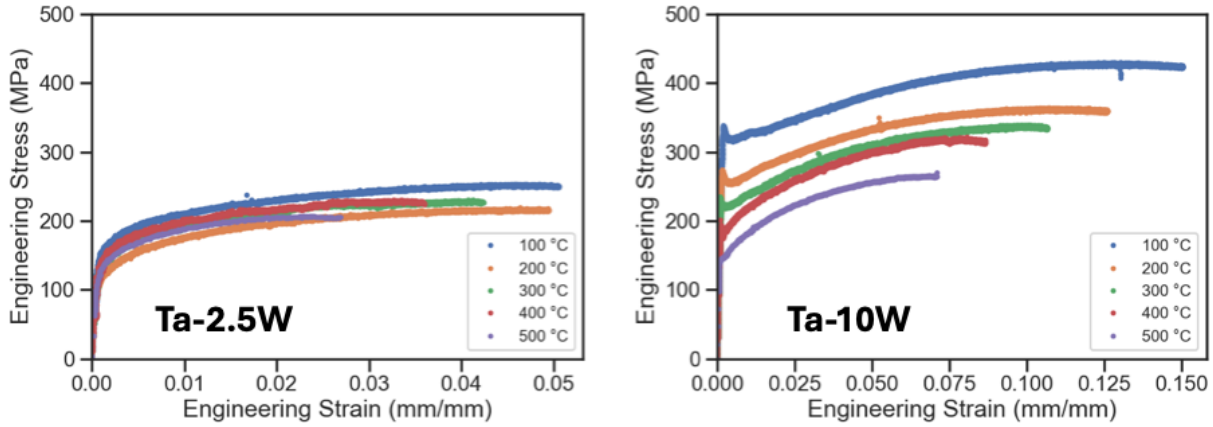

Figure 2.9: Engineering stress/strain plots for the Ta-2.5W (VM) and Ta-10W materials tested in uniaxial tension at temperatures ranging from 100 °C to 500 °C. These tests utilized the miniature tensile bar geometry for testing. The strain measurement used here is the crosshead displacement

3 Wrought Ta-W alloy plate characterization (dynamic)

3.1 Experimental approach (dynamic compression testing)

To gain an understanding of the effect of strain rate on dynamic behavior, mechanical tests were conducted with a compression split-Hopkinson pressure (Kolsky) bar at Mines. Experiments were performed using 12.7 mm diameter, 2.438 m long maraging steel bars. A 12.7 mm diameter, 203 mm long steel striker was fired at a pressure of 18 psi to compress samples to approximately 20% strain. A schematic of the dynamic compression experimental apparatus is shown in Figure 3.1. The resulting strain rates were on the order of 10^3 s^{-1} for the given striker length and pressure conditions. An annealed copper pulse shaper was used for each experiment to shape the incident pulse to obtain a constant strain rate.

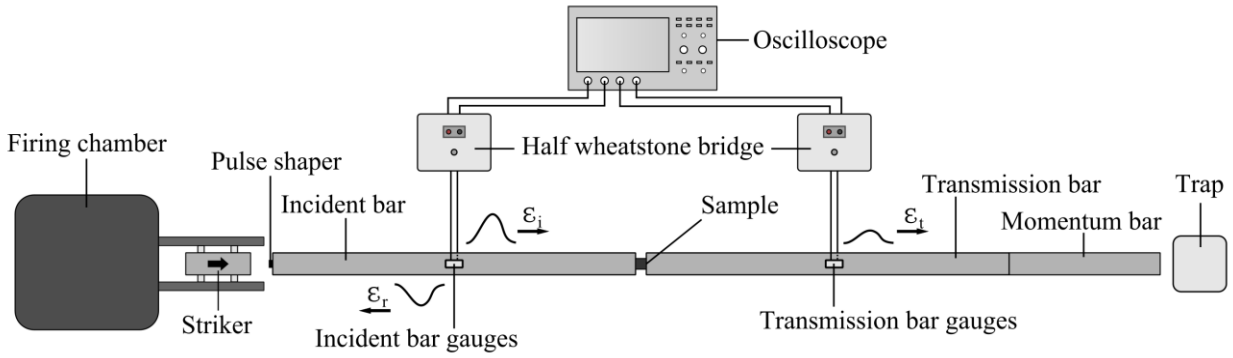

Figure 3.1: Dynamic compression experimental schematic.

Dynamic compression cylinders, nominally 5 mm diameter and 5 mm in length, were manufactured using EDM. The sample faces were polished to be parallel within 3 μm (deviation) to minimize friction effects at the striker bar/sample interface.

3.2 Results

3.2.1 Effect of tungsten alloy content on mechanical response

High-rate compression experiments were conducted on three different Ta-W alloy compositions with varying tungsten content: Ta-2.5W, Ta-5W, and Ta-10W. The resulting stress-strain behaviors are shown in Fig. 3.2.

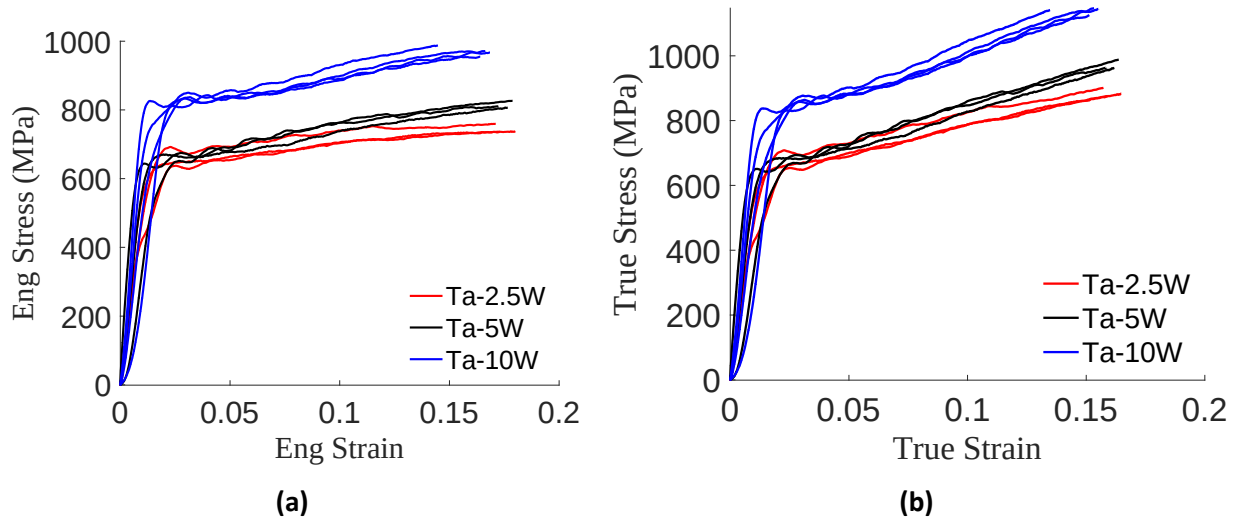

Figure 3.2: Engineering and true stress-strain dynamic compression behavior of Ta-2.5W, Ta-5W, and Ta-10W compressed at 25°C at an approximate strain rate of $2x10^3$ s^{-1}. These samples were machined from plate material supplied by VM (1/2" plate).

As W content increases, the yield and flow stresses are observed to increase. This is consistent with what has previously been observed in literature for Ta-W alloys tested under high-rates at room temperature [6,7,8].

3.2.2 Comparison of behavior in Ta-2.5W material from two vendors

A comparison of high strain rate, ambient temperature behaviors was made between Ta-2.5W provided by two vendors; American Elements and Viridis Materials (VM). The results are shown in Figure 3.3. The observed stress-strain behaviors are similar for the two vendors.

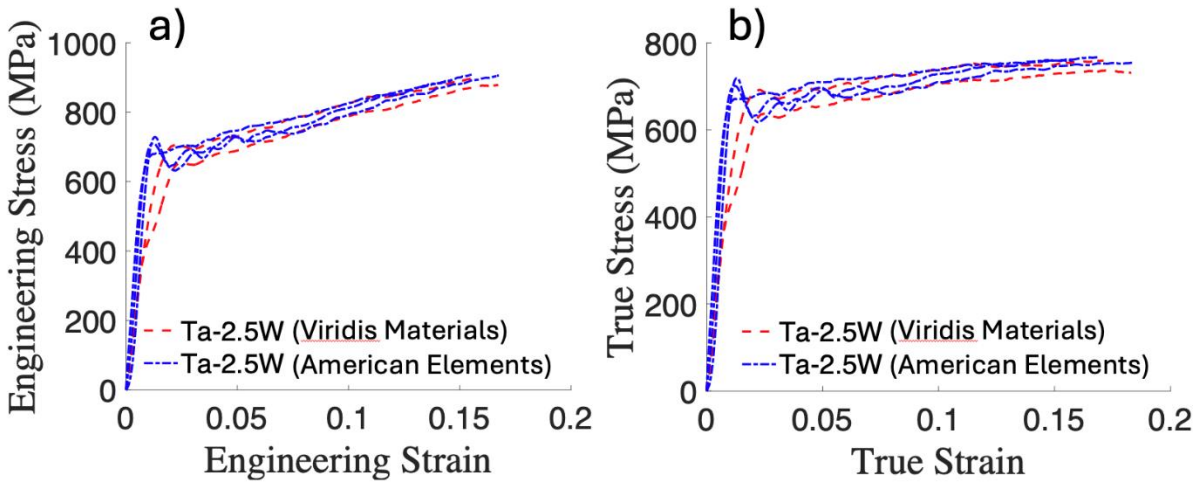

Figure 3.3: a) Engineering and b) true stress-strain dynamic compressive behaviors of wrought Ta-2.5W from American Elements (blue) and VM (red) tested at 25°C and an approximate strain rate of $2x10^3$ s^{-1}.

3.2.3 Effect of grain size on mechanical properties

To obtain material with varying grain sizes, heat treatments were conducted on compression test specimens machined from Ta-2.5W plate material (American Elements) at 1500 °C and 1800 °C for 2 h. Electron backscattered diffraction (EBSD) was performed to determine grain sizes. The 1500 and 1800 °C heat treatment conditions resulted in an order of magnitude grain size difference, with approximate average grain sizes of 45 μm and 400 μm, respectively. Representative microstructures, represented as inverse pole figure (IPF) maps, are shown in Figure 3.4.

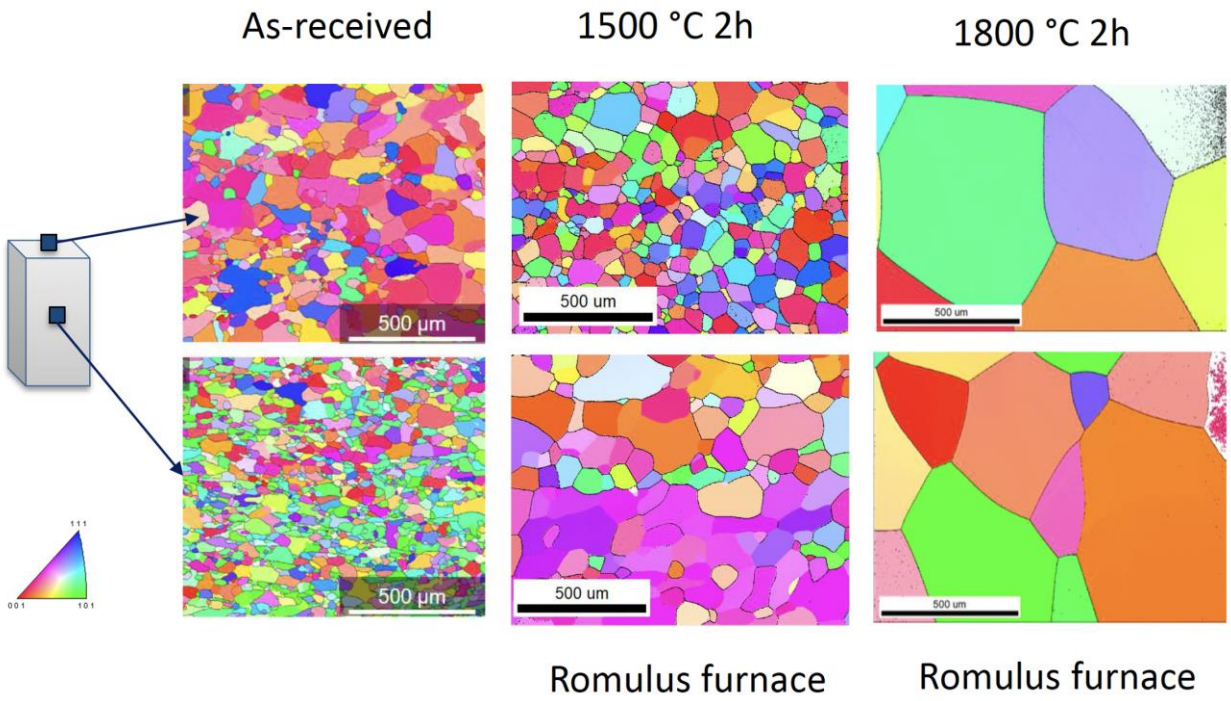

Figure 3.4: Non-deformed grain size comparison for as-received and heat treated microstructures of Ta-2.5W (American Elements).

Room temperature dynamic compression experiments were conducted on the heat-treated samples to evaluate the effects of grain size on the mechanical response. The results are shown in Fig. 3.5.

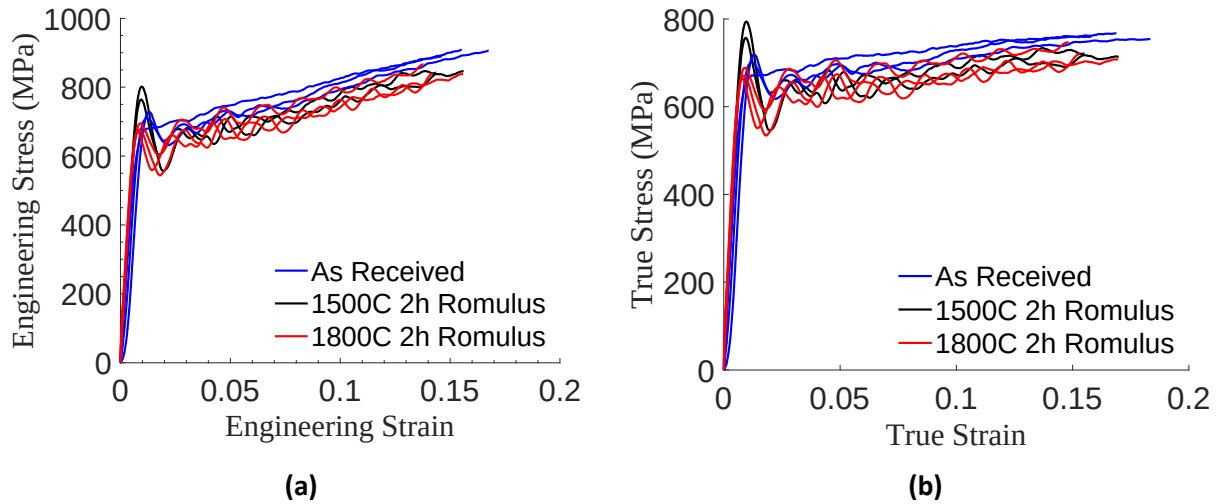

Figure 3.5: Dynamic compressive behavior of Ta-2.5W in the as-received, 1500 °C – 2h, and 1800 °C – 2h heat treatment conditions.

The high-rate response was similar across the two grain sizes, with both the 1500 °C and the 1800 °C conditions showing a similar reduction in yield stress from the as received condition. Both heat treatment conditions also demonstrated similar flow stress behaviors. However, the deformed microstructures indicated different deformation mechanisms may have been grain size dependent. Significant deformation twinning was observed in the 400 μm grain size material (1800 °C – 2 h), with some deformation twinning present in the 45 μm grain size samples (1500 °C - 2 h). The post-deformed microstructures are shown in Fig. 3.6.

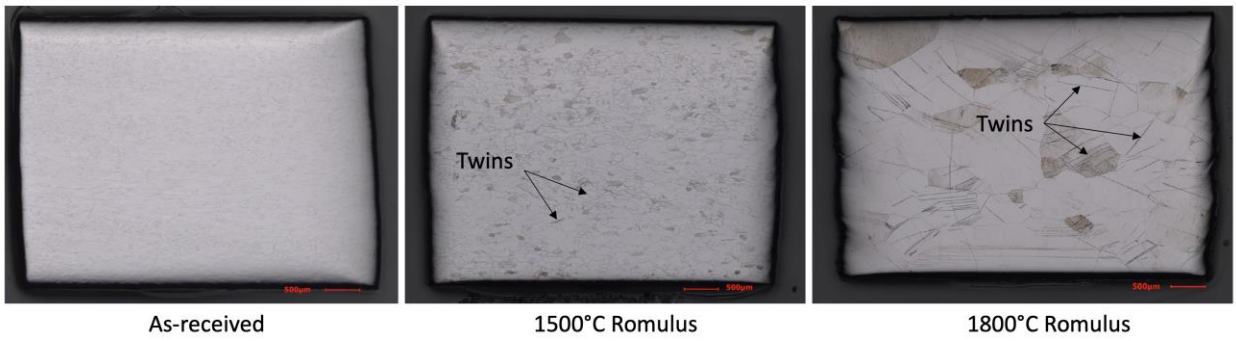

Figure 3.6: Deformed microstructures of the as-received and 1500 and 1800 °C, 2 h heat treatment conditions tested at an approximate strain rate of 2500 s^{-1} and a temperature of 25 °C.

3.2.4 Effect of impurities introduced during heat treatments

Two different 1500 °C heat-treatment conditions were performed using two furnaces: “Romulus” and “Nero”. The “Nero” 1500 °C heat treatment is believed to have introduced impurities, while the “Romulus” treatment is not believed to have. An investigation into the purity from each condition is currently being conducted. A comparison of the resulting stress-strain behaviors is shown in Fig. 3.7.

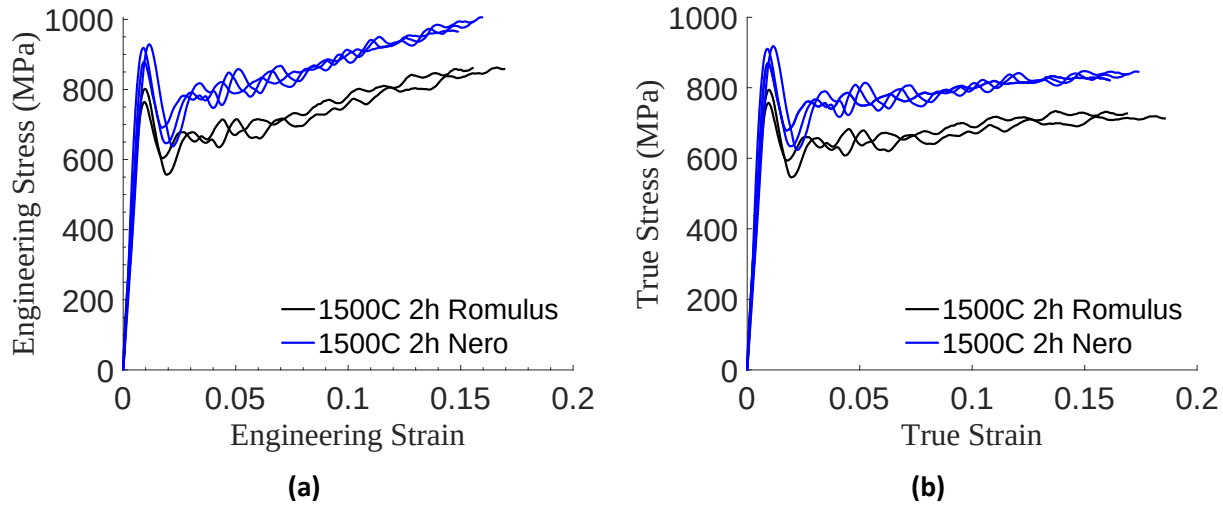

Figure 3.7: Dynamic compressive behavior of Ta-2.5W from two different 1500 °C heat treatment conditions at a strain rate of approximately 2500 s^{-1} and temperature of 25 °C.

The “Nero” heat treatment resulted in an increase in the yield strength compared to the “Romulus” heat treatment, which is speculated to be attributed to a combination of grain size and impurity effects, though a more thorough investigation is needed to quantify the resulting impurities for these two heat treatment conditions.

3.2.5 Effect of texture

The introduction of W can result in significant texture in wrought Ta-W plates. This has been observed previously in literature [4,6]. To investigate the effect of texture direction on the mechanical behavior, samples were machined along and perpendicular to the texture direction. The resulting stress-strain behavior is shown in Fig. 3.8.

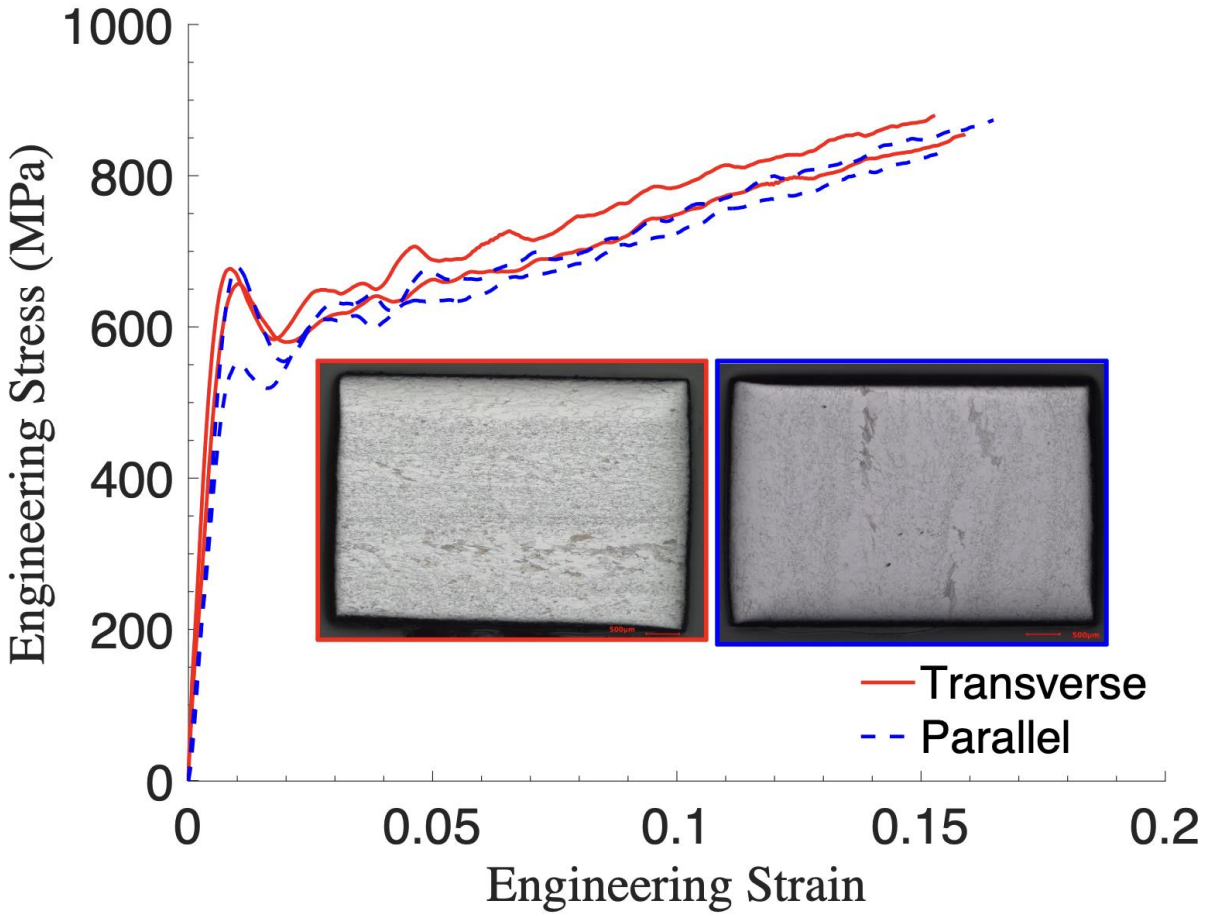

Figure 3.8: Dynamic compressive behavior of Ta-2.5W loaded transverse and parallel to the texture direction at a strain rate of approximately 2500 s^{-1} and temperature of 25 °C.

The resulting stress-strain behavior was similar for samples loaded along and transverse to the texture direction, with similar observed yield and flow stress behaviors for the two orientations. These results suggest that loading direction with respect to texture may not be a driving factor in the dynamic compressive mechanical response.

3.2.6 Effect of temperature on the mechanical properties in Ta-10W

To investigate the combined effects of temperature and strain rate, experiments were conducted on Ta-10W (legacy LLNL material) at temperatures of 25 °C and 400 °C. The resulting stress-strain behaviors are shown in Fig. 3.9.

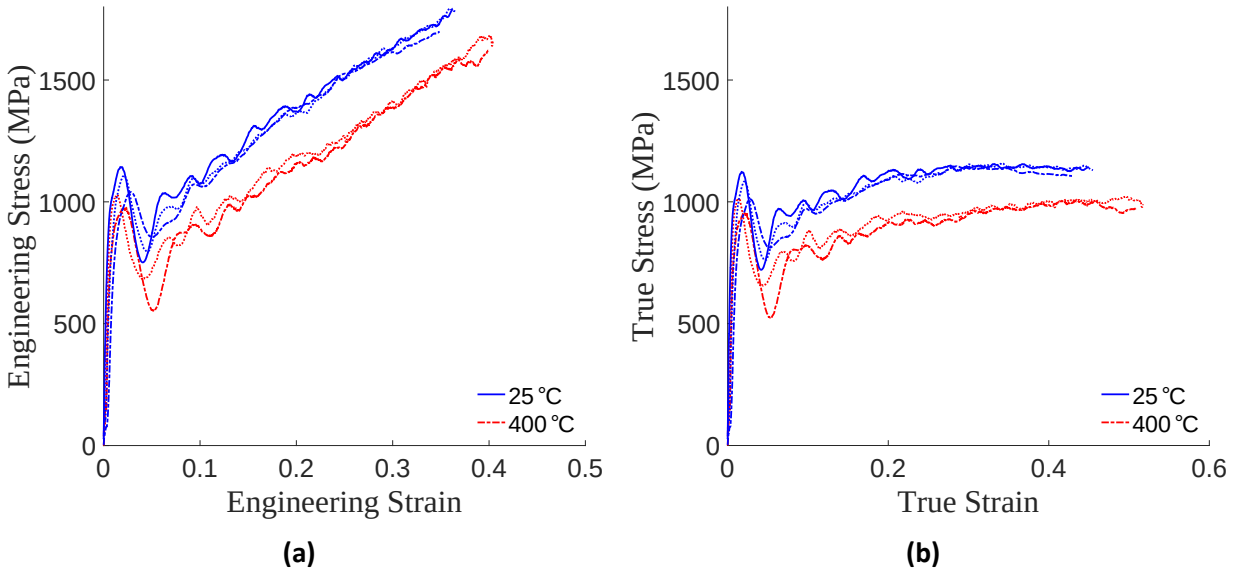

Figure 3.9: Dynamic stress-strain behavior of Ta-10W at 25 °C and 400 °C.

Ta-10W demonstrates lower yield and flow-stresses at higher temperatures. The dependence of flow stress on temperature demonstrates a significant decrease. The stress-strain behavior observed is like what has been observed by other authors who have conducted studies involving high rate, high temperature compressive deformation behavior of Ta and Ta-W alloys [5,7,8,9].

4 Laser powder bed fusion (LBPF) Ta-2.5W characterization

4.1 Experimental approach

AM Ta-2.5W material made at LLNL was supplied to Mines for characterization and testing. An initial set of builds were provided, from two different powder feedstocks. The primary differentiation between the two powder feedstocks was the oxygen content, which are referred to here as High-O and Low-O, respectively. Small samples (~5 g) from each of the three initial builds were sent out to an external vendor for compositional analysis, including interstitial (C, N, O) analysis. Three additional builds (15 mm x 15 mm x 30 mm) printed using the powder with higher O content were also sent to Mines for machining of small mechanical testing samples. Table 4.1 lists the dimensions of the builds provided to Mines for characterization and testing. The density of builds A-C were verified using Archimedes density measurements.

Table 4.1: Table listing of AM Ta-2.5W builds supplied to Mines.

Build	Height	Width	Length	Feedstock powder	Density	Use
A	15	15	15	"High-O"	99.2 ± 0.3%	Characterization
B	15	15	15	"Low-O"	99.2 ± 0.2%	
C	28	15	15	"High-O"	98.6 ± 0.3%	Compression cylinders
D	28	15	15	"High-O"	~99% (est.)	
E	28	15	15	"High-O"	~99% (est.)	Micro tensile bars
F	28	15	15	"High-O"	~70% (est.)	Not used

For mechanical testing, two sample geometries were EDM sectioned out from builds C-E (High-O). 5 x 5 mm cylinders were made from builds C and D with the compression axis of the cylinder aligned along the build direction (BD) and transverse direction, respectively. Microtensile test specimens were machined out of build E; the sample geometry was designed such that samples with the tensile axis along the BD and transverse direction could be machined out from the same build. The geometry of the microtensile test specimen is shown in Figure 4.1. Compression testing at room temperature was performed using the Gleeble 3500 thermo-mechanical simulator at Mines. Tension testing was performed on a MARK-10 ESM1500 electromechanical load frame at Mines. Strain measurements were performed using a stereo DIC setup, as shown in Figure 4.2. The samples were prepared for DIC by first grinding away the EDM recast layer using 1200 grit SiC paper, followed by cleaning with isopropyl alcohol. A base layer of white high temperature ceramic-based spray paint was applied and allowed to dry, followed by a careful application of the speckle pattern using black high temperature ceramic-based spray paint.

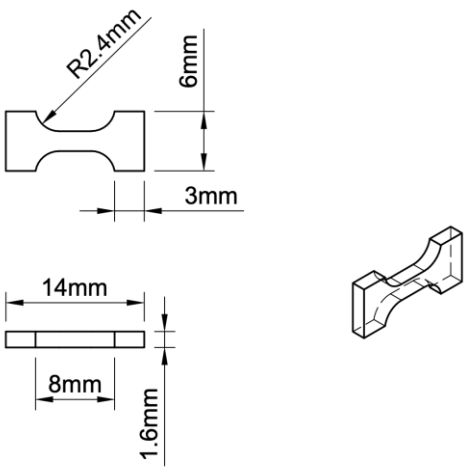

Figure 4.1: Microtensile bar sample dimensions. This design was derived from the miniature tensile bar design shown in Figure 2.1. The total length was reduced to fit within the AM Ta-2.5W build dimensions, while allowing for bars to be machined along two orthogonal directions (BD and transverse)

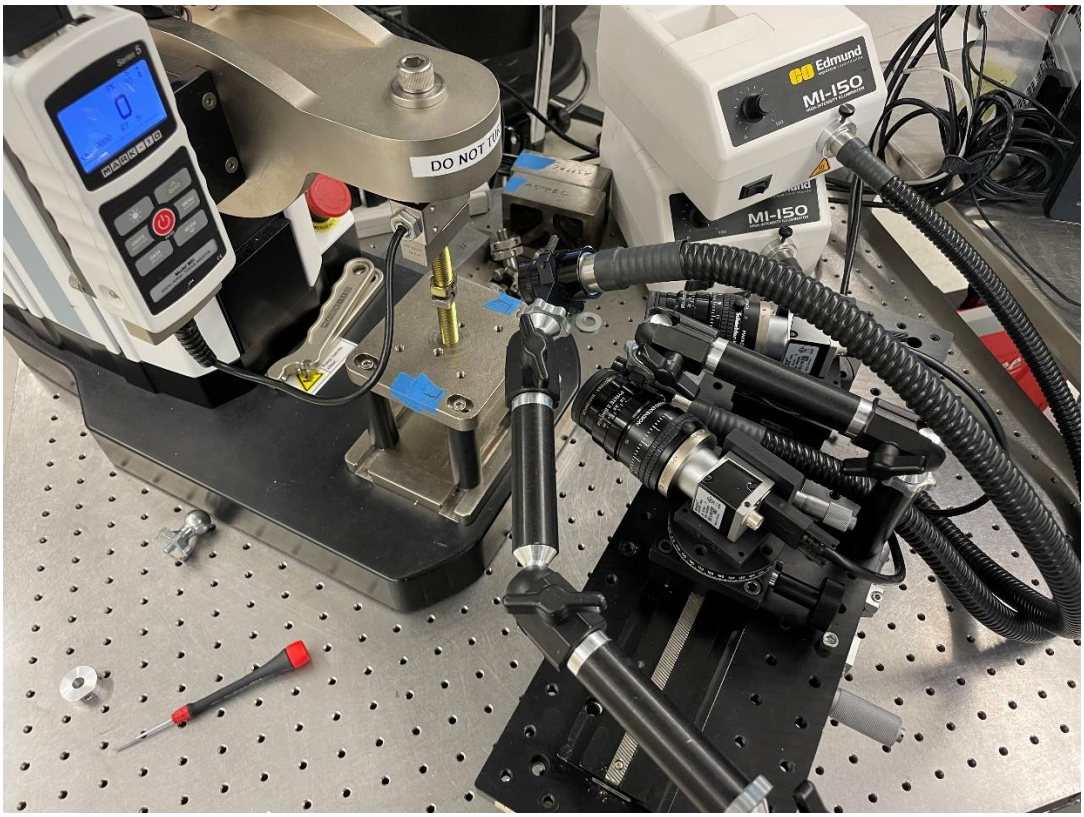

Figure 4.2: Stereo DIC set up used to test the micro-tensile samples on the MARK-10 load frame.

Fractography and EBSD were performed on a Tescan S85252G SEM/FIB. EBSD scans were taken near the fracture surface to relate grain orientation and morphology to fracture behavior. All the EBSD scan data were subjected to a grain dilatation cleanup that removes incorrect points or noise by expanding surrounding grains.

4.2 Results

4.2.1 Microstructure

Build A was sectioned into two pieces and mounted such that all three orthogonal faces were available for observation with either light optical microscopy or electron microscopy. An inverse pole figure (IPF) map of the microstructure is shown in Figure 4.3. The IPF map is oriented such that the crystallographic directions are shown with respect to the BD.

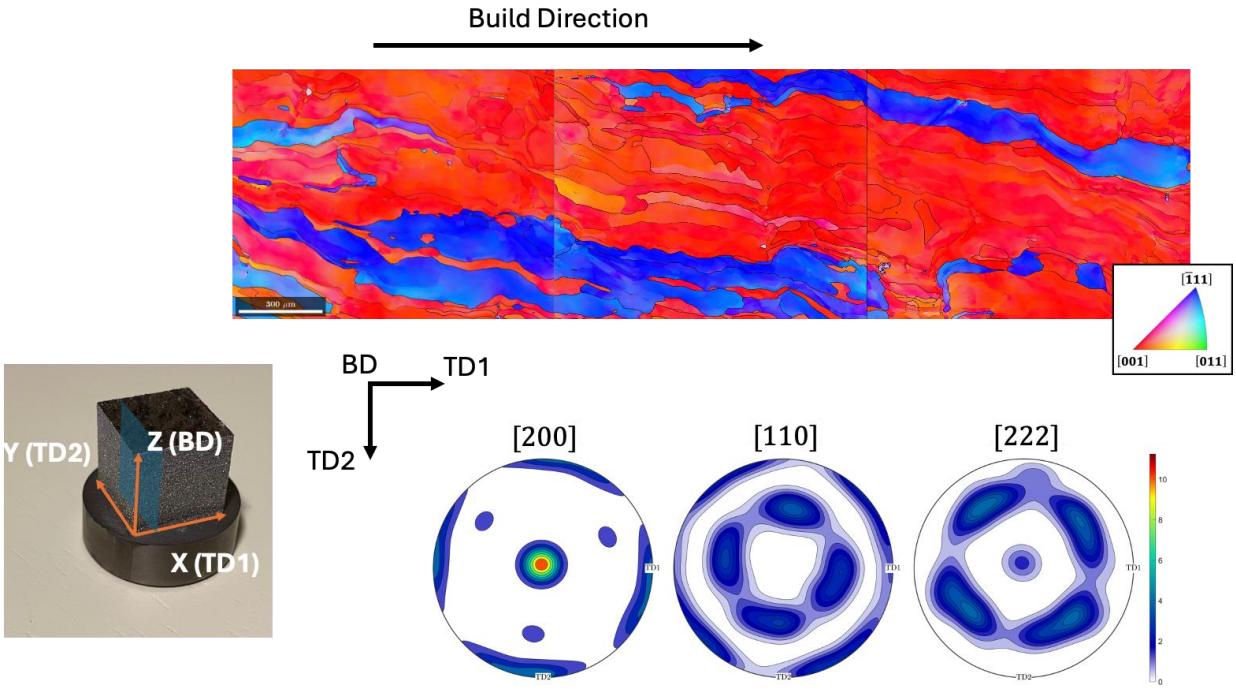

Figure 4.3: Inverse pole figure map (*top*) and pole figures (*bottom*) taken from Build A of the Ta-2.5W material obtained from LLNL. A strong <100> fiber is observed to fully describe the macrotexture for these builds. The defined coordinate system is shown (*left*), which was used to contextualize the EBSD results.

4.2.2 Uniaxial compression mechanical tests

The uniaxial compression stress/strain response for the AM Ta-2.5W material is shown in Figures 4.4 and 4.5 for the quasi-static and dynamic strain rate regimes, respectively. The apparent yield strength is slightly higher than the wrought Ta-2.5W material, particularly for the samples aligned along BD. (shown in Figure 2.5). For each strain rate, three replicate tests were run. The tests appear to be consistent between the duplicate tests.

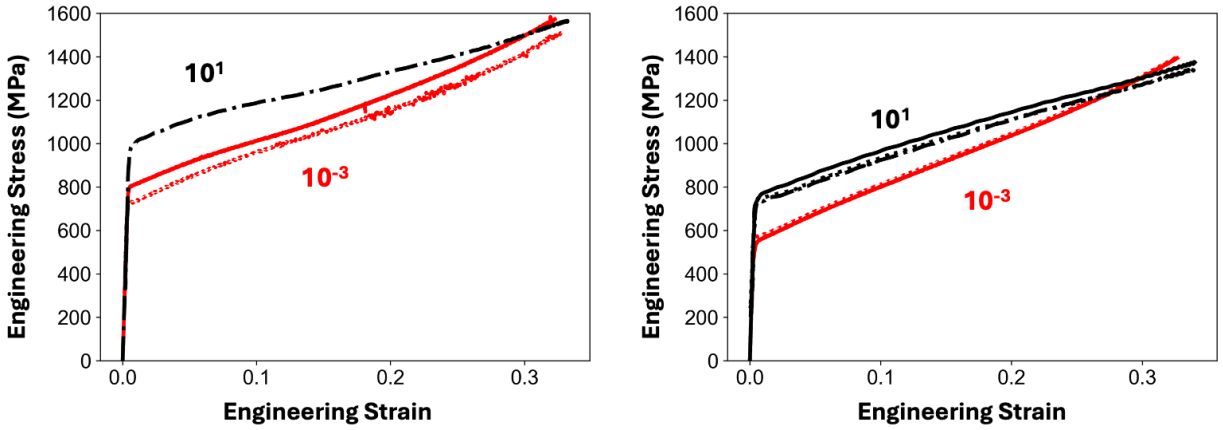

Figure 4.4: Engineering stress/strain plots for the Ta-2.5W AM material tested at two strain rates, 10^{-3} s^{-1} (red) and 10^{1} s^{-1} (black). The apparent yield strength is slightly higher than the wrought Ta-2.5W material, particularly for the samples aligned along BD. (shown in Figure 2.5).

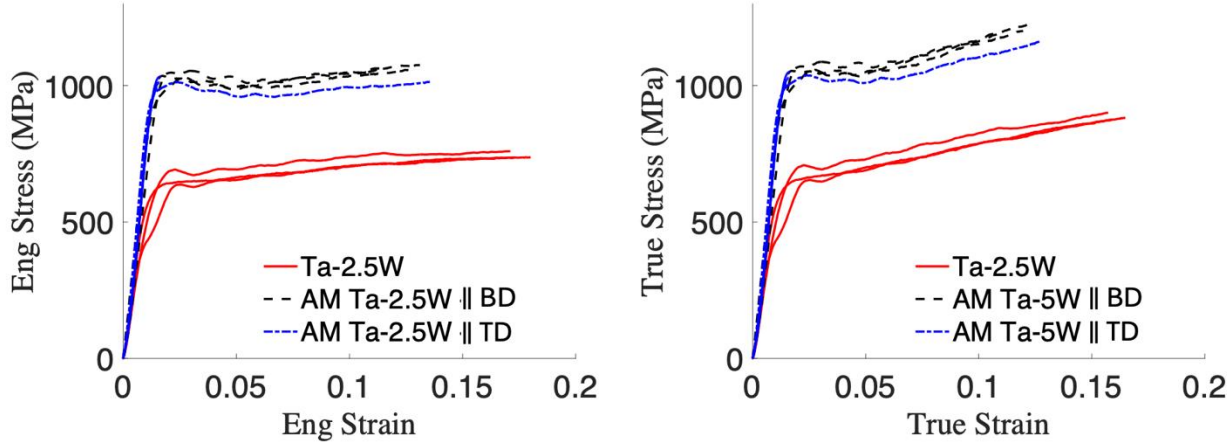

Figure 4.5: Engineering and true stress-strain dynamic compressive behaviors of AM Ta-2.5W and wrought Ta-2.5W compressed at 25 °C at an approximate strain rate of $2x10^{3}$ s^{-1}.

AM samples indicated higher yield stresses, regardless of orientation to the BD, when compared to the wrought material. An almost two-fold increase was observed between wrought and AM samples. Build direction did not have a significant impact on the resulting yield or flow behaviors at the dynamic strain rates tested here.

The deformed microstructures were also investigated using EBSD; the measured IPF maps for samples with the compression axis aligned with the BD are shown in Figure 4.6. The deformed microstructures did not exhibit evidence of deformation twinning, even in the dynamic compression tests. Grain reference orientation deviation (GROD) maps are shown in Figure 4.7, which show evidence of intergranular misorientation consistent with plastic deformation. The deformation microstructures are still under investigation for a future publication on the AM Ta-2.5W material.

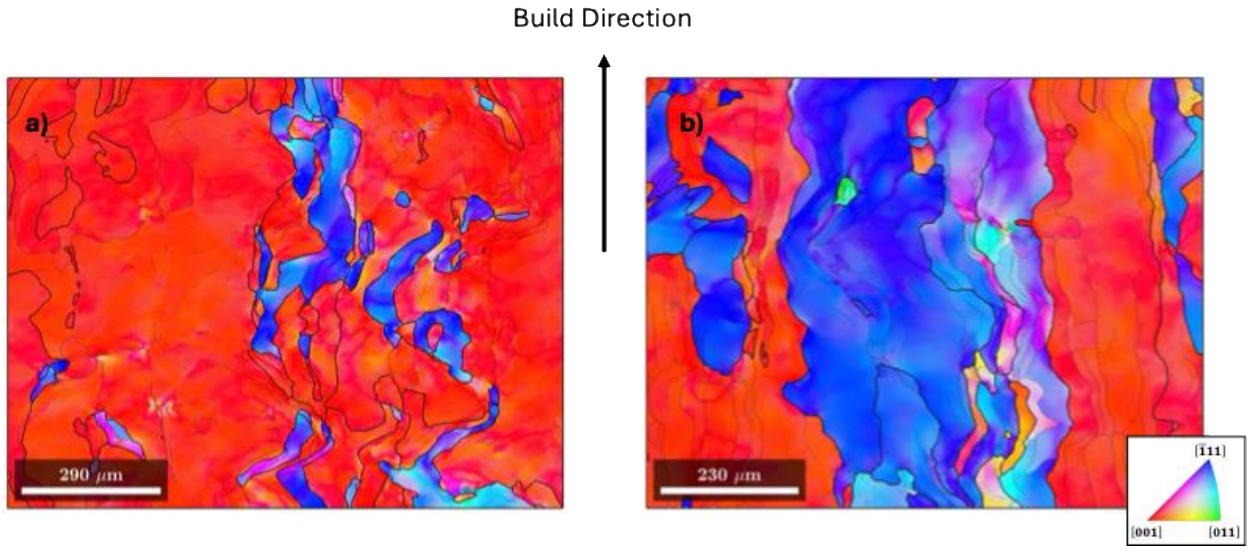

Figure 4.6: Inverse pole figure (IPF) maps of the deformed microstructure of the AM Ta-2.5W material (compression axis ‖ BD) at a) 10^{-3} s^{-1} and b) $2x10^{3}$ s^{-1}. The IPF maps are aligned to show the crystal orientation with respect to BD.

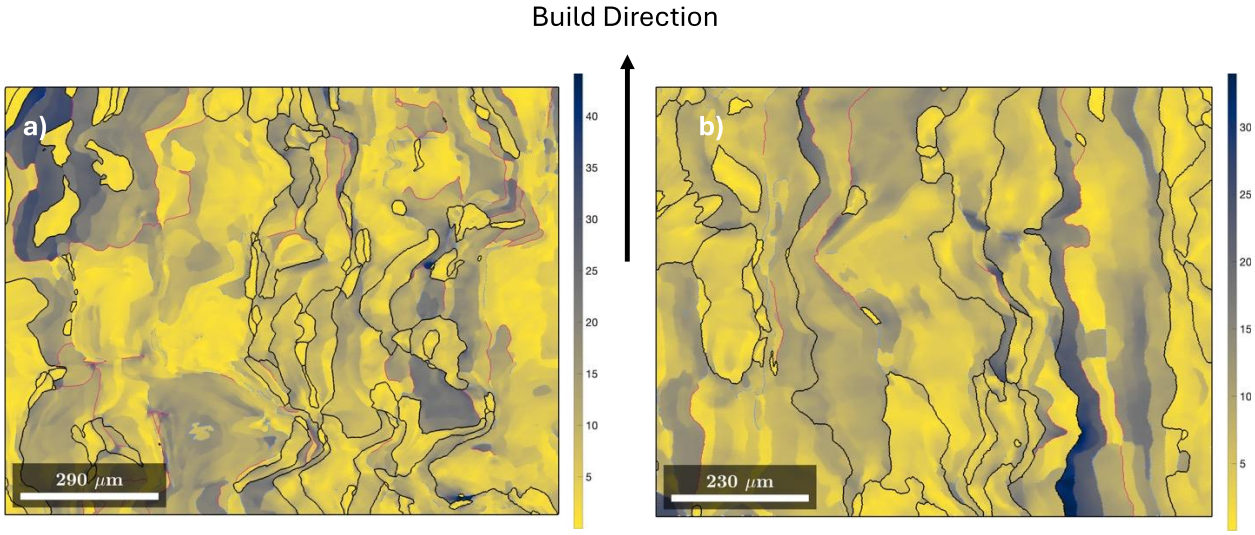

Figure 4.7: Inverse pole figure (IPF) maps of the deformed microstructure of the AM Ta-2.5W material at a) 10^{-3} s^{-1} and b) $2x10^{3}$ s^{-1}. The IPF maps are aligned to show the crystal orientation with respect to BD.

4.2.3 Uniaxial tension mechanical tests

Tensile tests were performed on samples extracted from the vertical and horizontal directions. The microtensile specimens were strained in displacement control at a nominal strain rate of 10^{-3} s^{-1} with a 2 Hz data/camera acquisition rate. The images were processed using Vic-3D (Correlated Solutions Inc., USA) to obtain displacement data across the gage section. Strain was extracted using a virtual

extensometer drawn along the gage length of each sample. The strain data was matched with load data by matching the drop in load with the fracture of the sample.

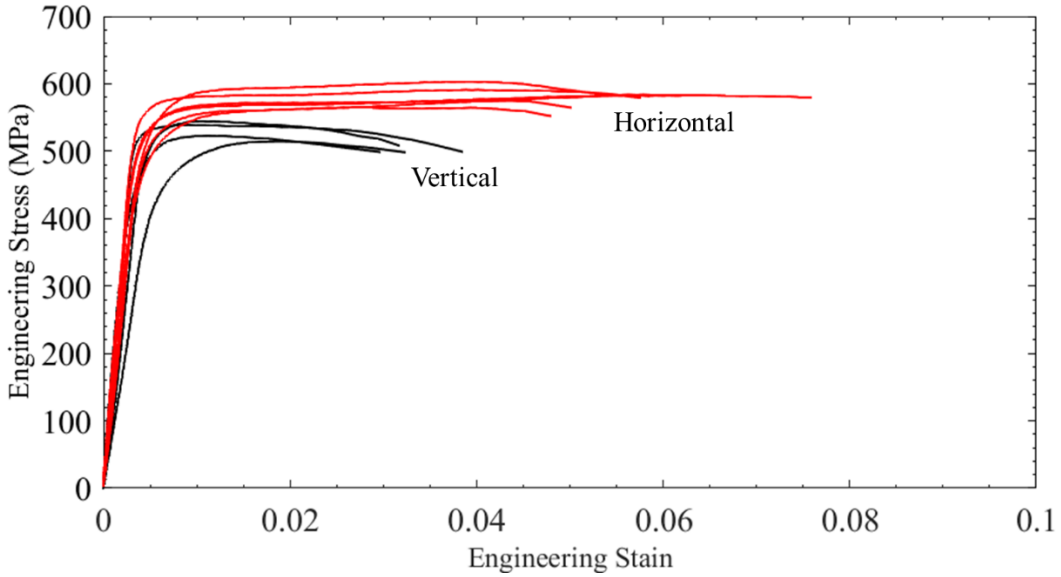

Figure 4.8: Engineering stress-strain plots of horizontal and vertical tensile bars (relative to the BD) displaced at a 10^{-3} s^{-1} strain rate.

Figure 4.8 displays stress-strain data for AM samples tested horizontal or vertical relative to the BD. The horizontal direction displays an increase in yield stress of about 50 MPa and an increase in total elongation compared to the vertical condition. Based on the fracture behavior, there was little to no apparent localized deformation (e.g., necking) and fracture occurred soon after the peak stress was achieved. Figure 4.9 displays localized strain across the gage length right before failure and Figure 4.10 displays the sample's cracking behavior as it fails. The local strain maps indicated a relatively even axial strain across the gage length, with localized areas of higher axial strain as secondary cracks formed. Due to the small size of the gage section, the speckle pattern created some gaps in the DIC data resulting from large spots of contrast. This should be a focus for improvement in future studies that utilize mechanical test specimens of this size (few mm).

Fractography was performed on a vertical and horizontal sample, as displayed in Figure 4.10. The fracture surfaces show different patterns, but display characteristic brittle fractures with no traces of shear lips forming. Large amounts of cracking are present on each fracture surface.

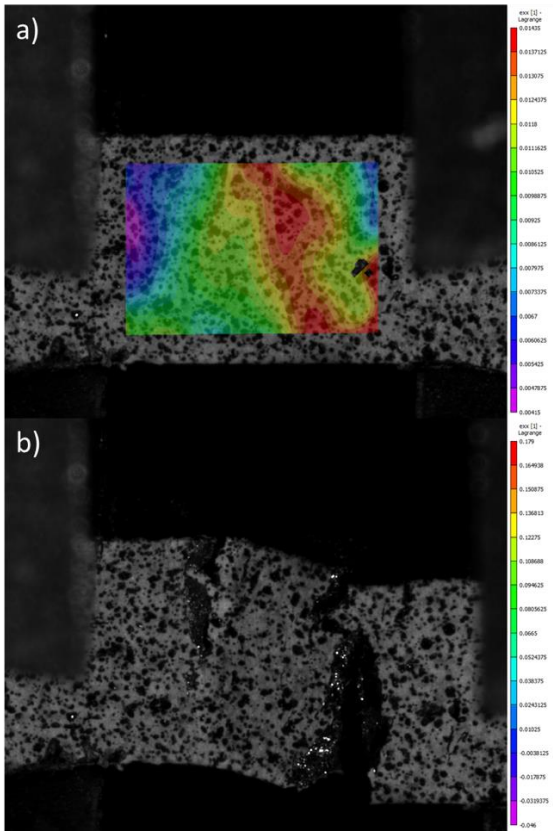

Figure 4.9: DIC strain topography map of a horizontal sample: a) localized strain that forms before fracture and b) the crack formation.

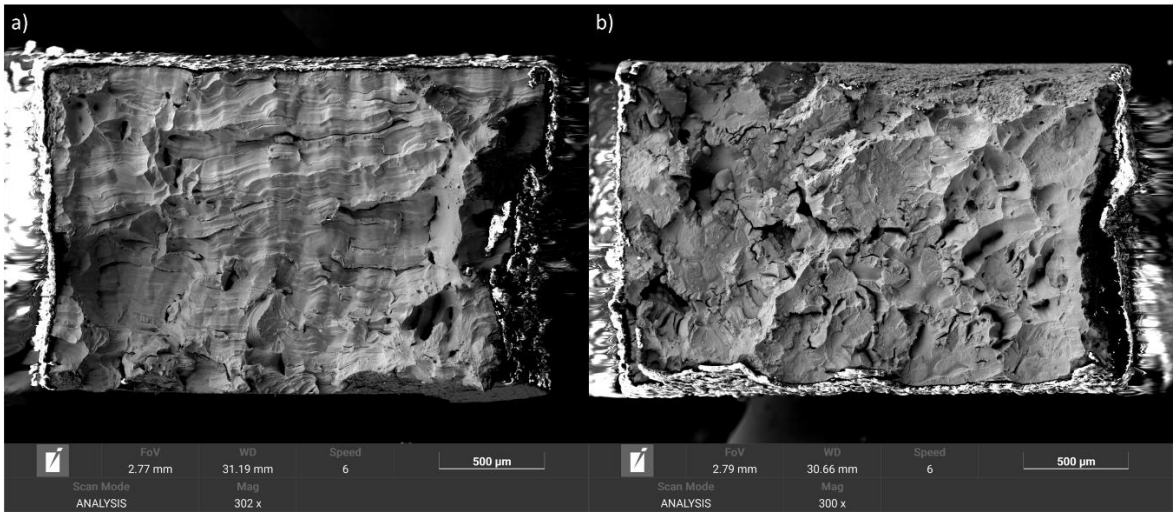

Figure 4.10: Fractography of a) a horizontal oriented sample and b) a vertical oriented sample.

EBSD was performed on the surface of fractured samples of both orientations and is displayed in Figure 4.11. Each map underwent a grain dilatation cleanup, and a grayscale IQ map was overlayed on the inverse pole figure map. Elongated grains are present in the BD.

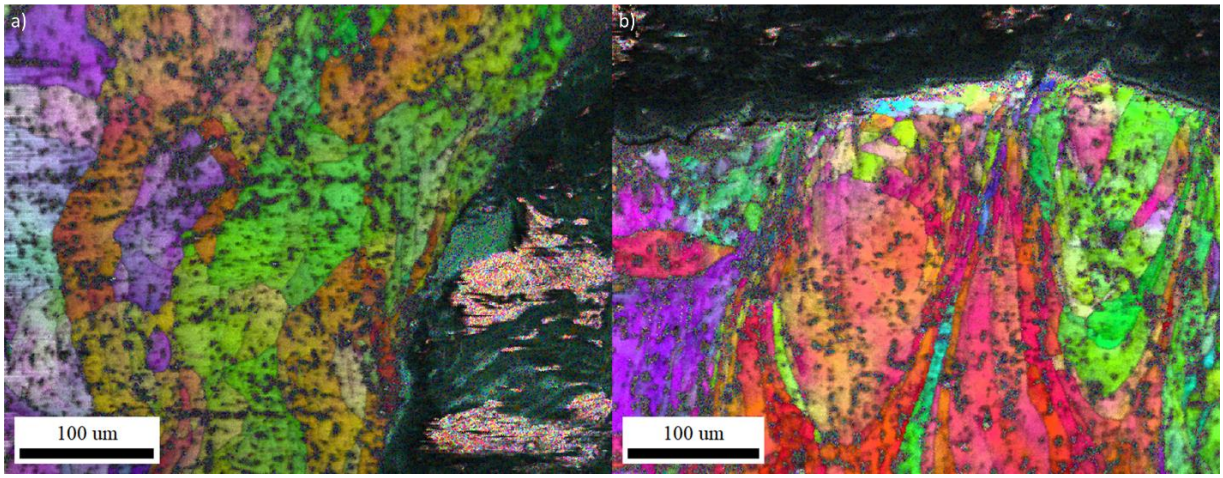

Figure 4.11: EBSD grain maps of the surface of a tensile bar at the fracture surface of an a) horizontal oriented sample and b) vertical oriented sample.

4.3 Discussion

The increase in elongation of the horizontal samples follows a common trend with AM orientation. The elongated grains that follow the BD act as large grains in the case of the horizontal direction; however, there is usually an increase in the yield and flow stress of the material when tested in the vertical direction or parallel to the BD. This trend is not observed in these tests, which suggests further exploration into aspects like defects may be warranted. The horizontal direction of the samples with the gage length perpendicular to the BD achieved higher yield and flow stresses and higher total elongations. The DIC images show failure mainly by cracks with no necking present. This indicates the fracture is mainly brittle with no shear components present. Secondary cracking is also present in some samples, further supporting brittle fractures. The failure mechanism seen in Figure 4.9b shows no necking, and the localized increase in strain observed by the processed DIC data may derive from the cracks that form. The overall strain field determined by the VIC3D shows a uniform strain field until the cracks start to form.

The fracture surfaces in Figure 4.10 support the conclusion made by the DIC images. Shear lips are not present in either the horizontal or vertical-orientated samples. However, the difference in the fracture surfaces is due to the orientational effects concerning the BD. Both orientations show some amount of (brittle) rock candy fracture, with the horizontal direction showing a wave-like fracture surface that could indicate interlayer/pass fracture.

The EBSD scans (Figure 4.11) show a typical AM microstructure. Grain elongation in the BD creates the anisotropic properties observed in the stress-strain data. The scans also show traces of internal porosity that are present. However, whether these pores and cracks are as-built or occur during the deformation process is unclear.

5 Summary

Project outcomes can be summarized as follows:

- Initial microstructure characterization of wrought plate material was performed, which revealed the wrought plates supplied by VM had significant amounts of unrecrystallized regions. Unrecrystallized regions were also observed in the legacy Ta-10W material supplied by LLNL, but the extent of these regions was not significant enough to affect the assessment of mechanical properties.
- YPE was observed in uniaxial tension testing of the wrought material (all three alloys), which is hypothesized to be caused by interstitials (O, C, N) present in the material. An improved high temperature testing setup in the Gleeble, with combined DIC and IR thermal imaging was used, with initial testing performed to validate the procedure. This setup allows for the measurement of strain within the gage section, while also observing any thermal gradients across the sample during displacement. By combining these two modalities, the strain in the uniform temperature portion of the gage section can be assessed.
- AM (laser powder bed fusion) Ta-2.5W material was received from LLNL for characterization and testing. The material was found to be nearly fully dense, with a strong crystallographic texture present; <100> fiber oriented along the build direction. The microstructure consisted of long (> 200 μm) columnar grains. The material had increased compressive strength when tested along both the BD and transverse directions when compared to the wrought 2.5W material. In tension, the material was found to have limited ductility along both directions, a significant decrease from the wrought Ta-2.5W material.

6 References

1. ASTM Standard E8/E8M-22, 2024, “Standard Test Methods for Tension Testing of Metallic Materials,” ASTM International, West Conshohocken, PA, 2015, DOI:1.1520/C0090-15
2. Ganapathy, M., et al. "A novel grip design for high-accuracy thermo-mechanical tensile testing of boron steel under hot stamping conditions." *Experimental Mechanics* 58 (2018): 243-258.
3. Mayerhöfer, Thomas G., et al. "CaF2: An Ideal Substrate Material for Infrared Spectroscopy?." *Analytical Chemistry*92.13 (2020): 9024-9031.
4. A.J. Schwartz, D.H. Lassila, M.M. LeBlanc. "The effects of tungsten addition on the microtexture and mechanical behavior of tantalum plate." Materials Science and Engineering: A, 1998, 244:178-190, doi: 10.1016/S0921-5093(97)00690-4
5. S.R. Chen and G.T. Gray, “Constitutive behavior of tantalum and tantalum-tungsten alloys,” Metallurgical and Materials Transactions A, 1996, 27: 2994–3006, doi: 10.1007/BF02663849.
6. G.T. Gray, S.R. Bingert, S.I. Wright, S.R. Chen, “Influence of tungsten alloying additions on the mechanical properties and texture of tantalum,” MRS Proceedings, 1993, 322: 407, doi: 10.1557/PROC-322-407.
7. S. Nemat-Nasser and R. Kapoor, “Deformation behavior of tantalum and a tantalum tungsten alloy,” International Journal of Plasticity, 2001, 17:1351–1366, doi: 10.1016/S0749-6419(00)00088-7.
8. J. Zhou, A.S. Khan, R. Cai, L. Chen, “Comparative study on constitutive modeling of tantalum and tantalum tungsten alloy,” Journal of Iron and Steel Research International, 2006, 13: 68–74, doi: 10.1016/S1006-706X(06)60081-2.
9. M. Knezevic, I.J. Beyerlein, M. L. Lovato, C.N. Tomé, A.W. Richards, R.J. McCabe, “A strain-rate and temperature dependent constitutive model for BCC metals incorporating non-Schmid effects: application to tantalum–tungsten alloys,” International Journal of Plasticity, 2014, 62: 93–104, doi: 10.1016/j.ijplas.2014.07.007.